SSIM 2023 – PM Dight (ed.)

doi:10.36487/ACG_repo/2335_35

Exceptional travel distance for a Pilbara failure

DG Ross *BHP, Australia*

Abstract

A 140,000 m^3 slope failure occurred in a BHP Western Australia Iron Ore mine in the Pilbara region. This occurred in Cenozoic sediments and the Archean West Angelas Member of the Marra Mamba Iron Formation. The 80 m high failure occurred on a slope of 50° measured from pit crest to slope toe and resulted in a deposit runout of 133 m. This exceeded the 95th percentile Whittall (2015) Fahrböschung model travel distance prediction of 124 m. Individual particles travelled to 152 m. This runout behaviour was significantly beyond the author's 12-year experience in the Pilbara iron ore environment. As the scale of iron ore mining in similar geological settings in the Pilbara is considerable, the intention is to share this runout behaviour for the benefit of the surface geomechanics community and particularly those operating in this environment. This case history outlines elements of the failure geometry, geology and hydrogeology. It then reconciles the runout against the Whittall (2015) Fahrböschung Volume model and the Optimised Mobility Index model. Whether the runout models are suitable for this environment and whether Pilbara Cenozoic and West Angelas materials are more mobile than the Whittall (2015) Fahrböschung dataset are discussed. Other observations are included, such as how runout estimates based on the moving surface area might change rapidly where failures expand rapidly. Lastly, the lack of groundwater data from within the slope and potential limitations, even if it had been present, is also discussed.

Keywords: *runout, Fahrböschung, Pilbara*

1 Introduction

Towards the end of the wet season in 2021, there was a slope failure in a BHP Western Australia Iron Ore mine in the Pilbara region. The failure debris pile runout was 133 m and exceeded the 95th percentile prediction interval of the Whittall (2015) Fahrböschung Volume model.

The failure was duly reported as a fall of ground event to the Government of Western Australia Department of Mines, Industry Regulation and Safety. It was also the subject of post-failure stability analyses as part of an internal investigation, with recommendations adopted.

There is a very large-scale of iron ore mining in the Pilbara region in similar geological settings. The purpose of this paper is mainly to communicate the runout behaviour to those such as Rio Tinto and Fortescue Metals Group operating in this particular environment.

This paper focuses on a back-analysis of the failure runout distance. The runout models were not used pre-failure. Strength back calculations, mechanical properties, validation of trigger action response plans and monitoring practices are out of scope.

Elements of the failure geometry, geology and hydrogeology are covered. Actual runout is reconciled against the Whittall (2015) Fahrböschung Volume model and the Whittall (2015) Optimised Mobility Index. Also discussed is whether the Pilbara Cenozoic and West Angelas materials are more mobile than the Whittall (2015) dataset. Illustration is provided with regard to how runout estimates based on the area of surface movement may change rapidly where failures expand rapidly. In addition, the observation that debris scatter occurs beyond the predicted runout toe of the referenced models is reiterated, and seiches (tsunamis) are not covered.

The value in this work is its communication that the Whittall models may not be appropriate in this environment.

2 Failure geometry

Before failure, the slope was 84 m high, consisting of 24 m high double batters at 65° batter angle, 9.3 m berm widths, returning an inter-ramp design angle of approximately 49°, and a crest-to-toe angle of 50°. The pit floor was approximately 80 m wide on unblasted ground, before rising 4 m onto an unmined blasted flitch approximately 75 m wide (Figures 1 and 2).

The Fahrböschung angle (failure crest to farthest reach of the deposit, excluding individual boulders) was 21°. The deposit fan travelled 133 m from the slope toe at the farthest reach. Individual debris was scattered up to 152 m.

Failure height was 80 m, width approximately 150 m. Area on face and volume were approximately 14,000 m^2 and 140,000 m^3 respectively. A section through the failure shows a near vertical backscarp approximately 32 m high, with rill angle debris to the pit wall. Beyond the pit wall, the debris could be summarised as being near flat on average.

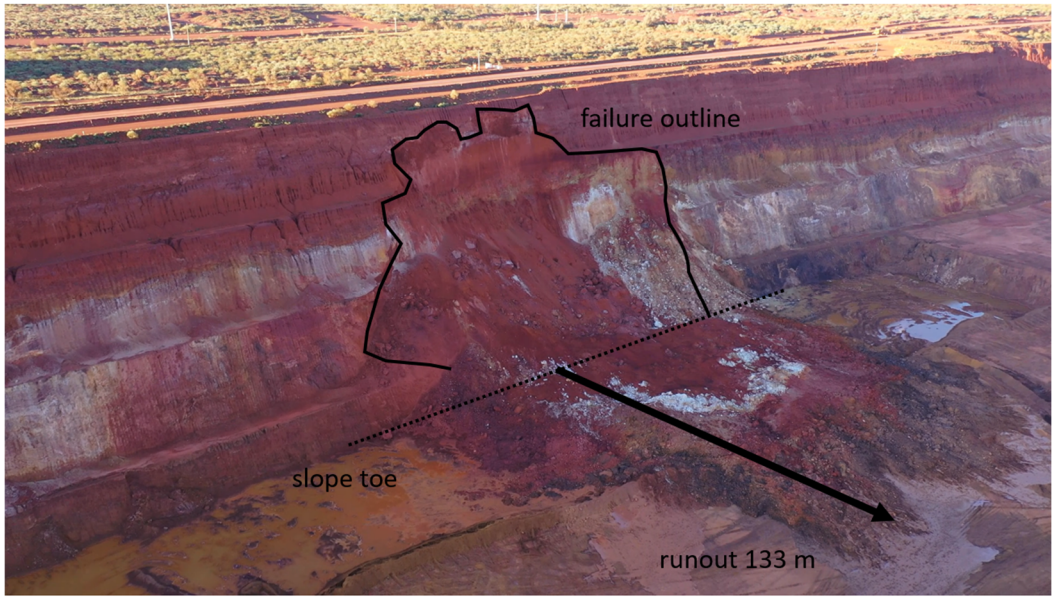

Figure 1 Failure image

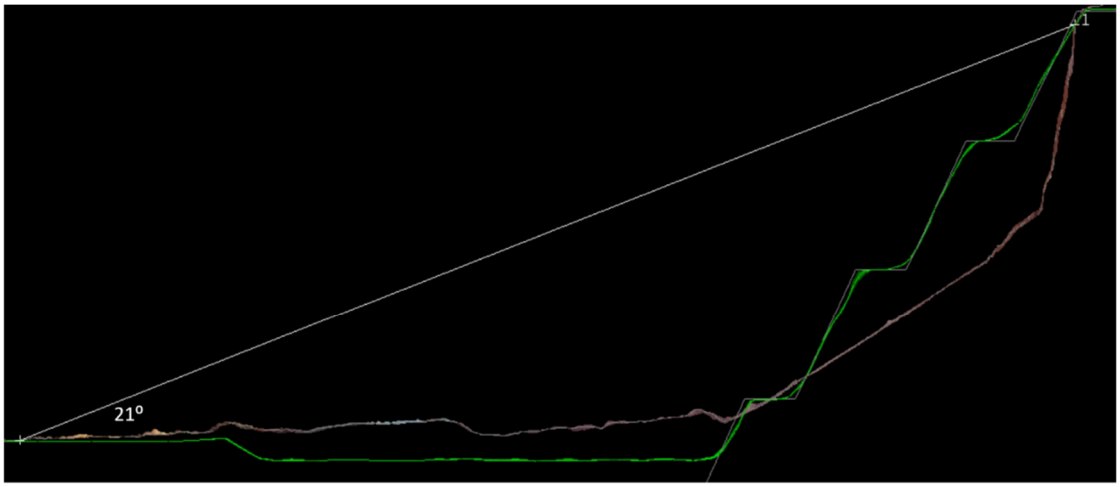

Slope Design:
Batter Height: 24 m
Batter Angle: 65°
Berm Width: 9.3 m
Chainage: 000 m

Failure:
Fahrboschung: 21°
Slope toe: debris toe:- 133 m
Slope toe: boulder scatter limit:- 152 m

Failure Height: 80 m
Failure Width: 150 m
Indicative Failure Depth: 14 m
Indicative Area on Face:- 14,000m^2
Indicative Failure Volume:- 140,000 m^3

Figure 2 Section chainage 000 m

3 Geology

The geology of the failure has been interpreted as Cenozoic sediments on weathered West Angela 2 shale unit of Archean age (WA2). The Cenozoicgeology is classified according to Baxter (2016) and is illustrated in elevation (Figure 3) and section (Figure 4). Generic mechanical properties for these units are outlined in Baxter (2016); however, these are not necessarily the same properties of the failed materials. In this case, these were mostly soil-like or a combination of soil and weak weathered rock.

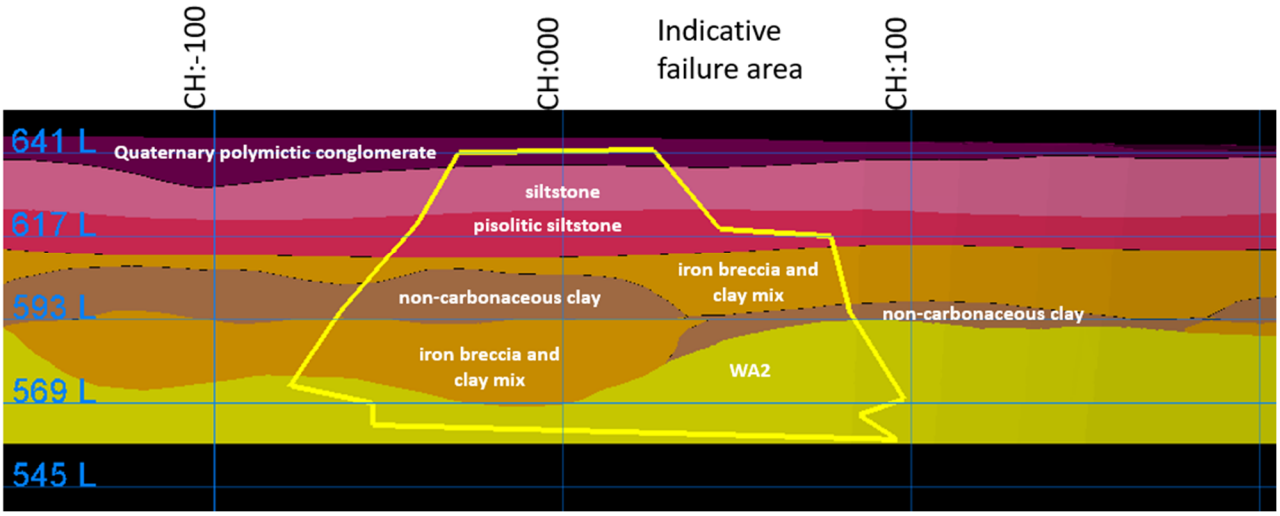

Figure 3 Interpreted geology of failure: elevation

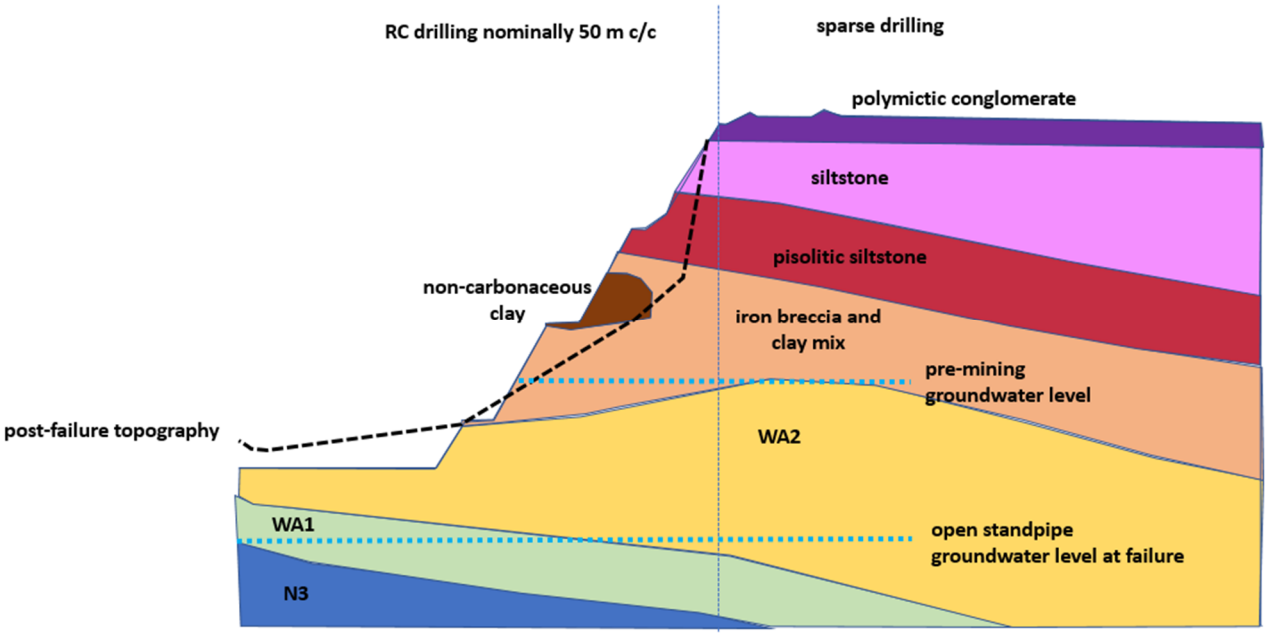

Figure 4 Interpreted geology of failure: section at chainage 000 m

From the base upwards, this shows the weathered West Angela 2 shale unit – iron breccia and clay mix with some non-carbonaceous clay within – successively covered by layers of pisolitic siltstone, a siltstone and polymictic conglomerate. Reverse circulation drill spacing to inform the geology model was nominally 50 m centre-to-centre in-pit and sparse ex-pit. Pre- and post-failure, lineaments were present in the upper batter, which are interpreted as near vertical faults (Figure 5).

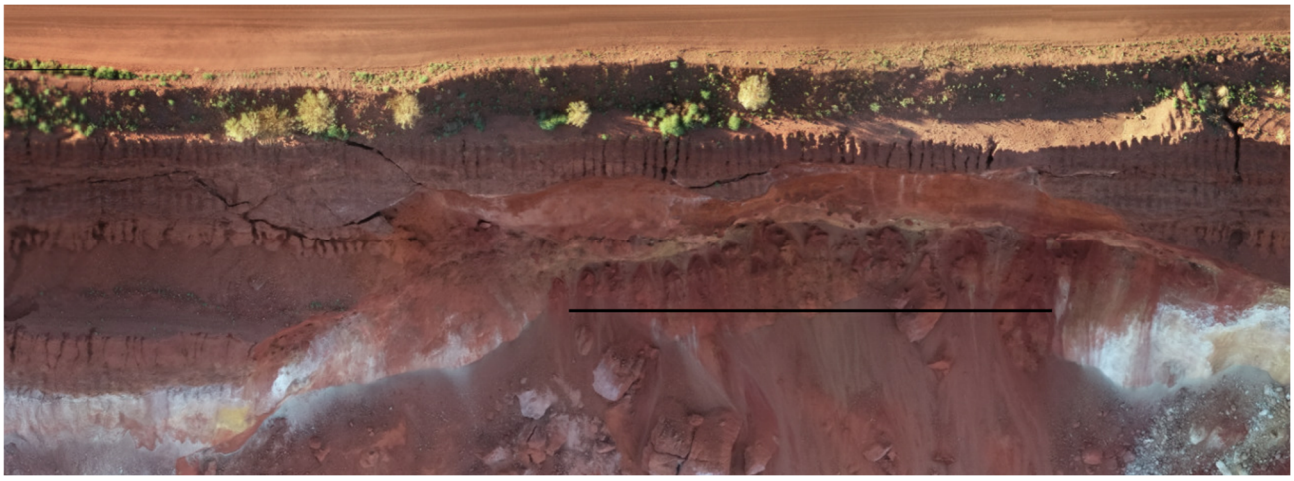

Figure 5 Plan view of lineaments in batter at crest of failure, interpreted as near vertical faults

4 Hydrogeology

4.1 Pre-mining

The orebody straddled the pre-mining water table. The pre-mining water table was at an elevation of approximately 63 m below ground surface (Figure 4). No contemporary vibrating wire piezometer data was available in the vicinity of the failure.

4.2 Leading up to failure

During mining, water was being managed by ex-pit pumping bores, as illustrated in Figure 6, and a low yielding in-pit bore. Open standpipes were located approximately 100 m behind the crest and spaced at approximately 500 m centre-to-centre in four locations. Pumping and static water levels in these were about 20 m below the pit floor at the time of failure (Figure 4).

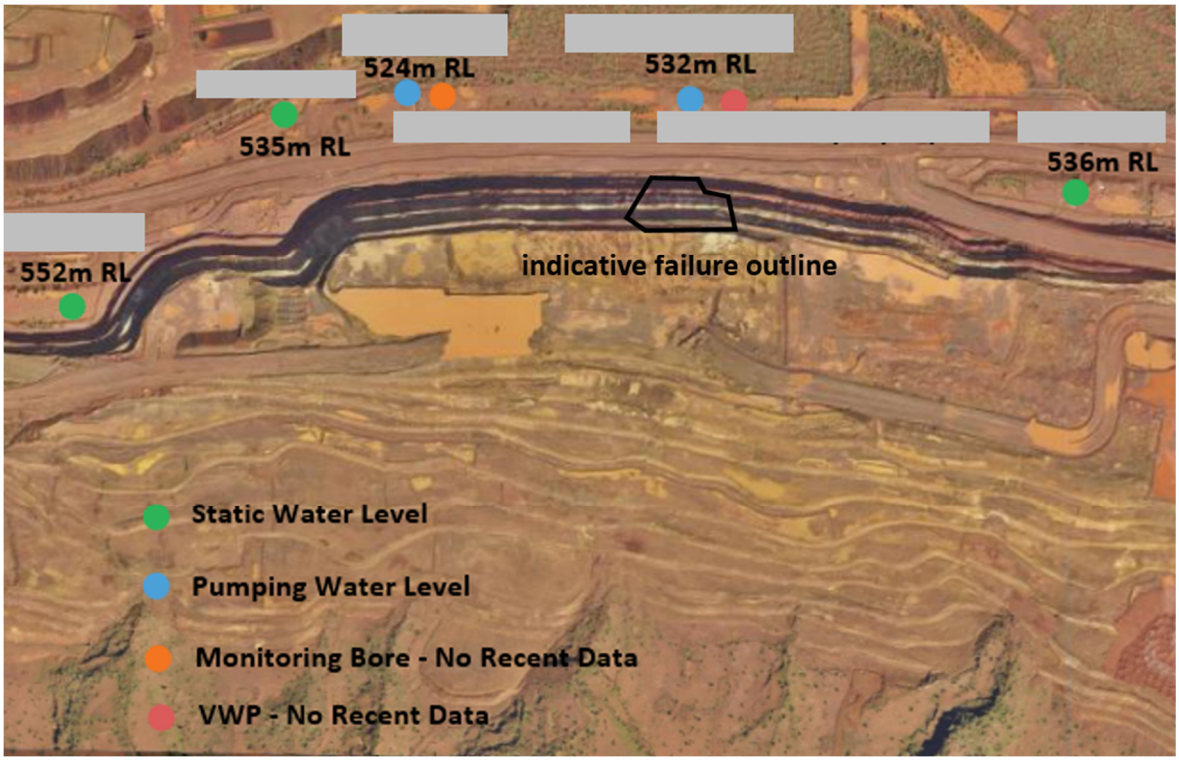

Figure 6 Groundwater observations

Seasonal rainfall and ephemeral streamflow is typical. The creek in the valley behind the pit had been tipped over. As is typical after large rainfall events, a large zone of surface water inundated the valley for a few weeks (Figure 6). This included ponding along the edges of the windrow at the slope crest and the haul road behind for some of the time. Surface water presenting at the pit floor was typically left to evaporate.

Local rainfall records show a one-in-five-year 24-hour rainfall event of about 112 mm occurring 64 days before failure. Approximately 75 mm of this occurred within one hour, exceeding the one-in-100-year magnitude for a one-hour event. A 53 mm one-in-two-year rainfall event occurred nine days before failure (Figure 7).

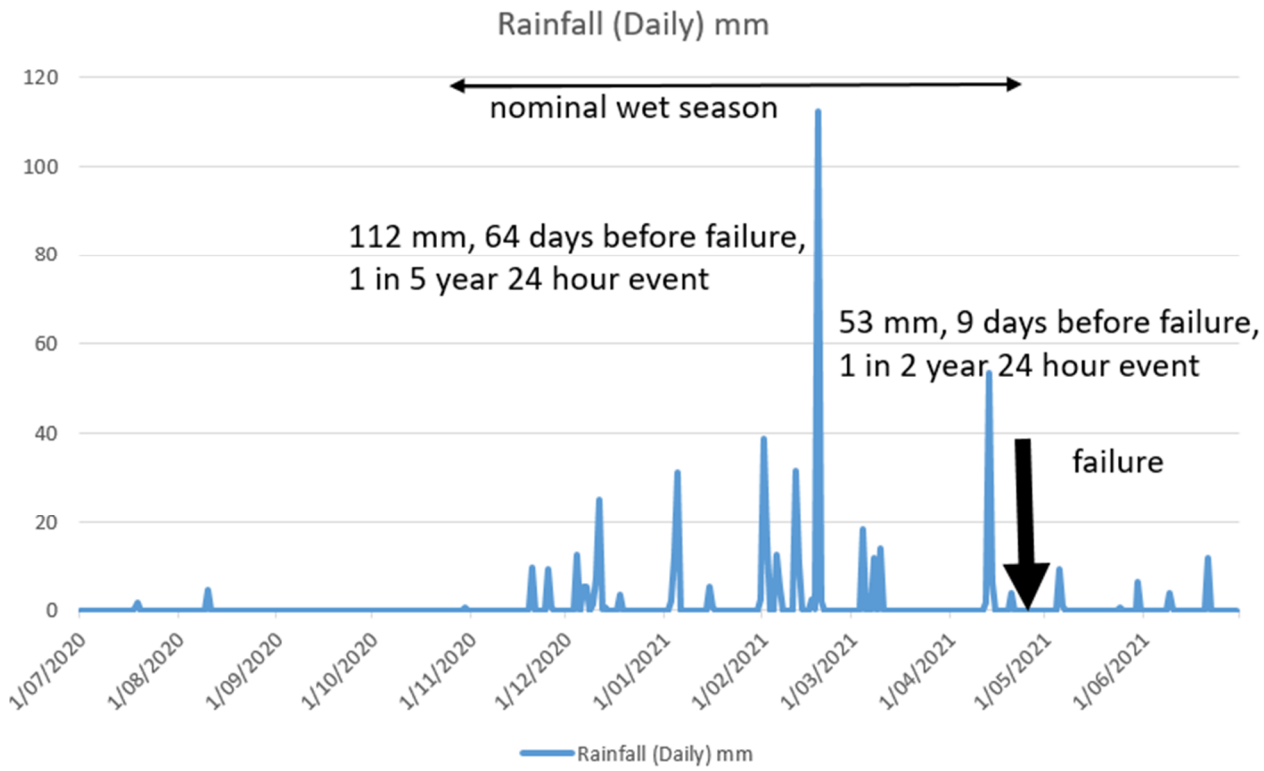

Figure 7 Daily rainfall (mm) in lead up to failure

It was known during mining that there were ‘wet pockets’ in ore and waste that were attributed to areas of poorer drainage and fed by wet weather events.

4.3 At failure

Dark areas on a photograph taken 24 hours before failure are interpreted as wet material or seepages up to the 580 RL (pre-mining water table). These are visible over an approximately 30 m length of the western side and an approximately 10 m length at the eastern side (Figure 8). At the time of failure, there was surface water on the pit floor, perhaps 10 cm deep, with some ‘islands’. The pit floor water is a remnant from the 53 mm rainfall event (Figures 1 and 8).

Figure 8 Failure area 24 hours pre-failure, showing reactivation of a previous double batter failure. Dark patches on walls interpreted as seepages. Surface water on pit floor inferred to be perhaps 10 cm, with some islands

5 Runout model reconciliation

This section focuses on reconciling against two runout models. These are the Fahrböschung Volume relationship (Whittall 2015) and the Optimised Mobility Index model (Whittall 2015). The Fahrböschung Volume model and the Optimised Mobility Index model (Whittall 2015) are based on a database of up to 105 open cut mine failures of which approximately 10% were soils. Minimum failure volume was 40,000 m3. All of the following text in Section 5.1 is based on Whittall (2015).

5.1 Fahrböschung Volume model and Optimised Mobility Index model (Whittall 2015)

Whittall (2015) states:

> *'A common empirical runout prediction method is the concept of the 'Fahrböschung' angle … to graphically describe runout as the inclination of the line that connects the crest of the main scarp to the toe of the deposit.'*

This is shown as Figure 9 where:

- H = vertical distance from crest of failure scarp to toe of deposit.
- L = horizontal length from crest of failure scarp to toe of the deposit.
- L_o = runout distance from the slope toe.

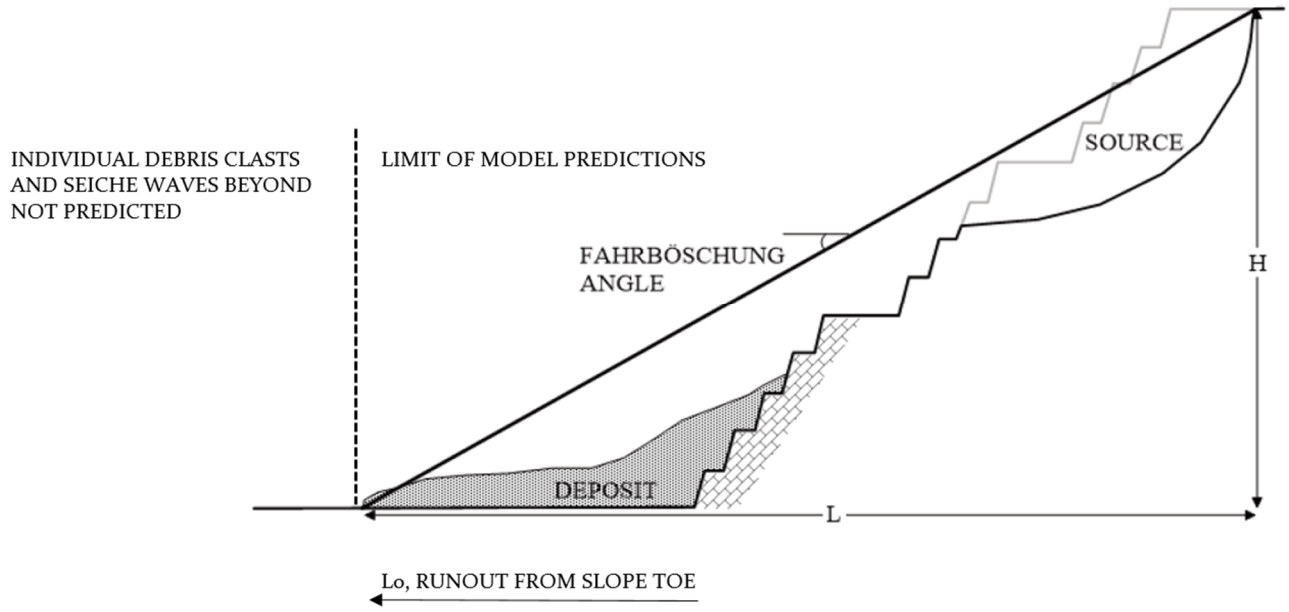

Figure 9 Whittall et al. (2020) schematic definition of the Fahrböschung angle, modified to show L_o (runout distance from the slope toe) and limit of model predictions

5.1.1 Estimating source volume

Source volume estimates are key inputs for both the Fahrböschung Volume model and the Optimised Mobility Index model. Whittall proposed a trend for prediction of failure volume based on deformation surface area based on 61 pit slope failure cases (Equation 1).

$$V = 0.238(surface\ area)^{1.407} \quad (1)$$

where:

V = volume

To generate this relationship, Whittall derived surface area post failure by the length through the centreline of the deformation from the toe of the rupture surface to its crest or the back-break. Width is the average of the maximum and minimum widths measured on the rupture surface. Surface area also can be estimated from radar monitoring in the lead up to failure (Dick et al. 2015 referenced in Whittall 2015).

5.1.2 Fahrböschung volume models

The Fahrböschung Volume models were derived by plotting H/L against failure volume. Two different material behaviour trends were proposed: one for the more mobile weathered weak rock and one for the less mobile fresh strong rock. The Fahrböschung Volume models for weathered weak rock and fresh strong rock are shown in Equations 2 and 3 respectively.

$$\log(\frac{H}{L}) = -0.138\log(volume) - 0.895 \quad (2)$$

$$\log(\frac{H}{L}) = -0.151\log(volume) - 0.587 \quad (3)$$

5.1.3 Optimised Mobility Index

Whittall found that fall height and slope angle are also important variables in addition to volume and proposed the Optimised Mobility Index trend to incorporate these. This model dataset includes both weak weathered rock and fresh strong rock material types. Whittall's schematic illustration of the inputs to this model is reproduced in Figure 10.

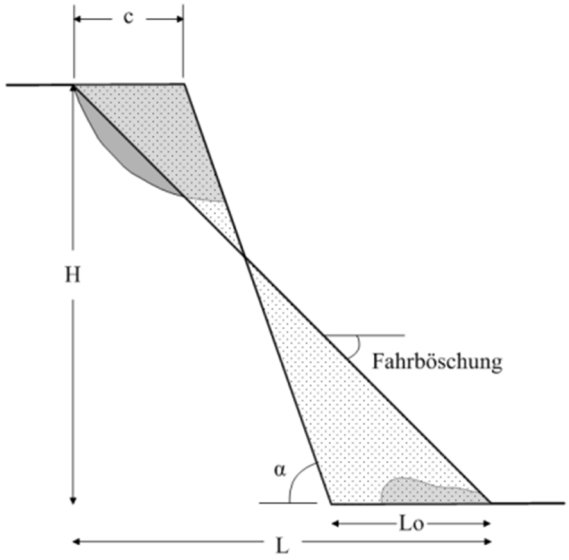

Figure 10 Schematic of Optimised Mobility Index geometry (Whittall 2015)

Whittall (2015) states:

> *'The area of the upper triangle is a function of the crest back-break, the slope angle, and the Fahrböschung angle (Equation 4). If material reaches the pit floor (Fahrböschung angle < slope angle) the second triangle is a function of the slope angle, Fahrböschung angle, and the fall height remaining below where the upper triangle intersects the wall (Equation 5). The areas are normalised to the square of the slope height to account for differently shaped triangles with the same area, Equation 6 is the cumulative cross-sectional area of the two triangles normalised to fall height.'*

$$A_{upper} = \frac{c^2 sin\beta sin(180-\alpha)}{2sin\,(\alpha-\beta)} \quad (4)$$

where:

A_{upper} = upper triangle area.

c = crest back-break.

α = slope angle.

β = Fahrböschung angle.

$$A_{lower} = \frac{[H^2+L^2-(\frac{c\sin(180-\alpha)}{sin(\alpha-\beta)})^2]\sin\beta\sin(\alpha-\beta)}{2sin\,(180-\alpha)} \quad (5)$$

where:

A_{lower} = lower triangle area.

Equations 4 and 5 are actually part of Equation 6.

$$Optimised\ Mobility\ Index = \frac{A_{upper}+A_{lower}}{H^2} \quad (6)$$

The trend for the Optimised Mobility Index is shown as Equation 7, and the associated equation for runout beyond slope toe as Equation 8. Runout length from slope crest is set out in Equation 9.

$$\frac{A}{H^2} = 0.384(volume)^{0.240} \quad (7)$$

$$L_0 = \frac{2(H^2)(0.384V^{0.240})-c^2 tan\alpha}{H-ctan\alpha} \quad (8)$$

$$L = L_0 + \frac{H}{tan\alpha} \quad (9)$$

5.1.4 Notes on models

The Fahrböschung Volume model is split into weak weathered rock mobile trends and less mobile strong fresh rock trends. The Optimised Mobility Index is based on both types. The Fahrböschung Volume model only has failure volume as an input, whereas the Optimised Mobility Index also has height, slope angle and back-break (Table 1). Slope angle influence tends to zero if the failure does not extend beyond the pit crest. Using this dataset, Whittall found that the Optimised Mobility Index was found to have lower scatter than other models, including the Fahrböschung Volume model.

Table 1 Inputs to Fahrböschung Volume model and Optimised Mobility Index model

Fahrböschung Volume model (Whittall 2015)	Optimised Mobility Index model (Whittall 2015)
Volume	Volume
/	Height
/	Slope angle and back-break (failures beyond crest only)

5.1.5 Application

The application of the models are to set stand-offs below moving slopes based on the estimated 95th percentile runout distance. In other words, at a location with a probability of <=5% of runout exceedance. The models do not predict rollout distances of individual debris pieces beyond the debris pile or seiche waves if failing into water.

Sensitivity analyses of –50%, +100% volume were recommended, and Whittall (2015) also stated that a short runout prediction does not provide justification for continuing to mine on or below the slope expected to fail.

5.1.5.1 Fahrböschung Volume relationship

For the Fahrböschung Volume relationship, volume can be estimated based on surface area (Equation 1).

Whittall (2015) plotted the trend of Equations 2 and 3 onto separate prediction interval design charts. The charts also show the 5% runout exceedance probability. By plotting the failure volume estimate, the tangent of the runout angle with 5% runout exceedance probability can be read off. Projecting this Fahrböschung angle from the crest of the moving area into the pit can be used to set a standoff.

5.1.5.2 Optimised Mobility Index

Similarly, Whittall (2015) plotted the trend for the Optimised Mobility Index (Equation 7) onto a prediction interval design chart. By plotting estimated failure volume, the Optimised Mobility Index value with 5% runout exceedance probability can be read off.

Whittall (2015) is not explicit about how to translate the Optimised Mobility Index value with 5% runout exceedance probability into standoff. Trial and error of various Fahrböschung angles and the corresponding values of H and L can be applied into Equations 4 and 5 until the Optimised Mobility Index matching the 5% runout on the design chart is identified in Equation 6. As above, projecting the Fahrböschung angle from the crest of the moving area into the pit can be used to set a standoff.

5.2 Reconciliation

5.2.1 Volume

Based on radar images in the lead up to failure, surface area was estimated at 14,000 m^2. Applying 14,000 m^2 surface area into Equation 1 for volume gives a figure of approximately 160,000 m^3, which is quite close to the actual failure volume estimate.

Actual volume of failure was estimated by taking sections at 50 m centre-to-centre through the pre- and post-failure topographies, estimating pre-failure and post-failure areas on each and extrapolating between sections. Pre-failure volumes were estimated at approximately 133,500 m^3 and post failure at 146,000 m^3. As the figures were close, an average estimated volume of failure of 140,000 m^3 was taken. This was taken as fit for purpose.

5.2.2 Runout

The 50th and 95th percentile predictions of the Whittall (2015) Fahrböschung Volume model for weak weathered materials and Whittall (2015) Optimised Mobility Index model are tabulated in Table 2.

Table 2 Fahrböschung Volume model and Optimised Mobility Index model estimates

Fahrböschung Volume model (Whittall 2015)	Optimised Mobility Index model (Whittall 2015)
50th percentile – 85 m	50th percentile – 40 m
95th percentile – 124 m	95th percentile – 61 m

These show 95th percentile estimates of approximately 61 m for the Whittall (2015) Optimised Mobility Index and approximately 124 m for the Whittall (2015) Fahrböschung Volume relationship.

Prediction design charts including 100% sensitivity to volume and actual failure behaviour are shown in Figures 11 and 12.

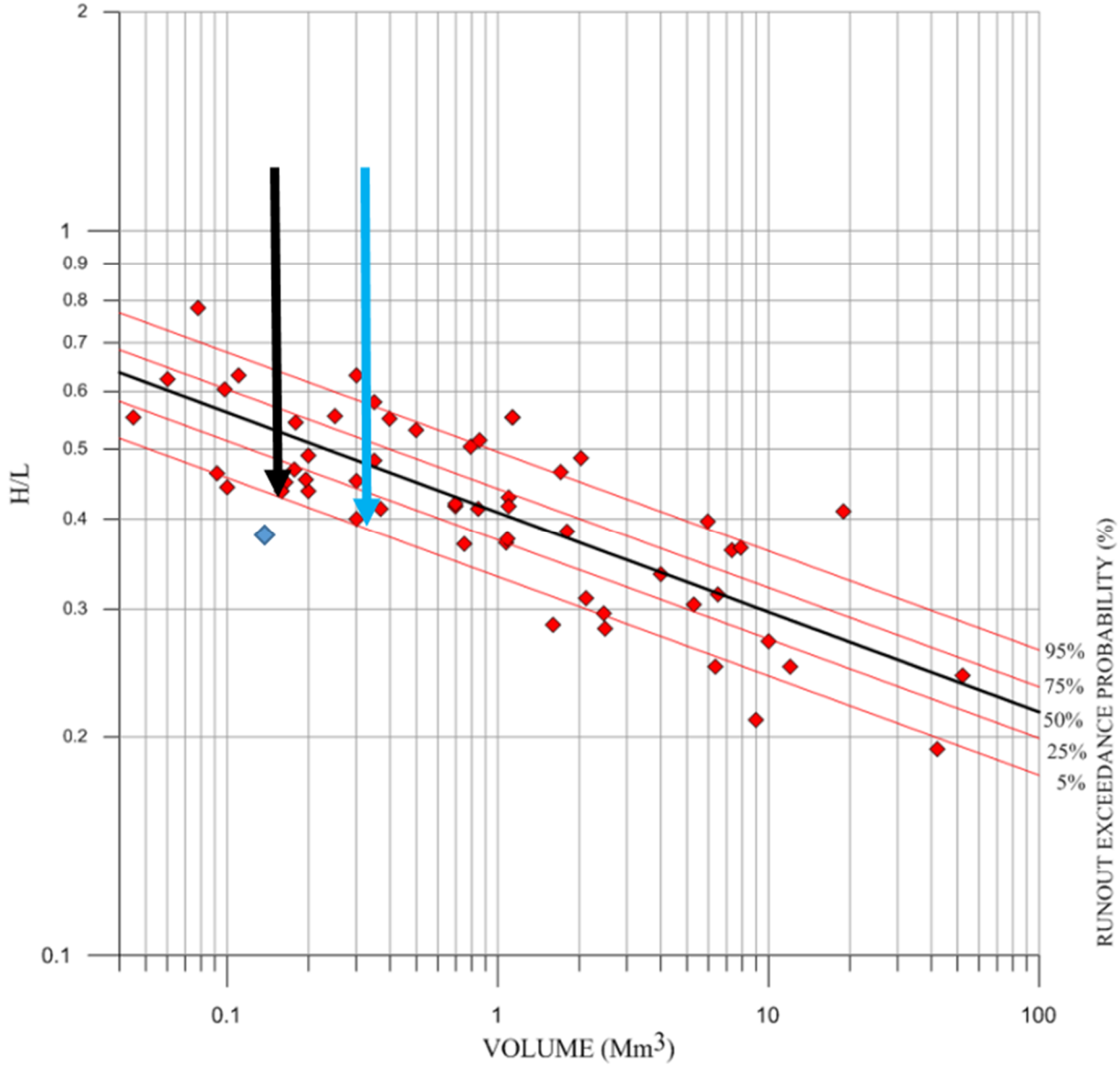

Figure 11 Whittall (2015) prediction interval design chart for the weathered weak rocks. Fahrböschung Volume relationship annotated by black arrow for a predicted 160,000 m³ failure volume and a 5% runout exceedance probability. Sensitivity of +100% volume shown by blue arrow. Blue diamond represents the actual 140,000 m³ failure, with a Fahrböschung angle of 21° (H/L = 0.385)

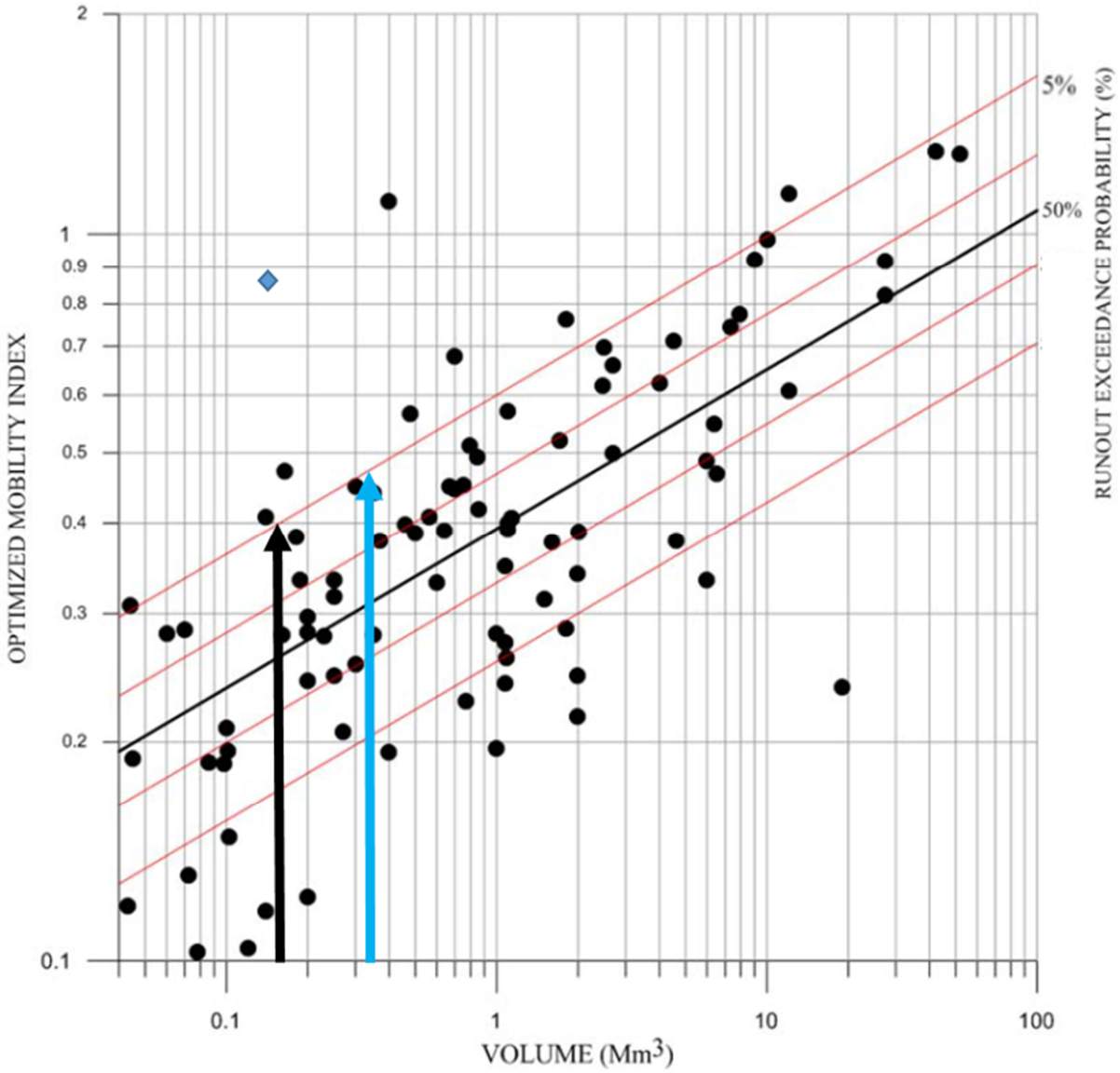

Figure 12 Whittall (2015) prediction interval design chart for the Optimised Mobility Index relationship annotated by black arrow for a predicted 160,000 m³ failure volume and a 5% runout exceedance probability. Sensitivity of +100% volume shown by blue arrow. The blue diamond represents the actual 140,000 m³ failure with an Optimised Mobility Index of 0.88. Note runout exceedance probability labels adjusted from Whittall (2015) original to reflect increasing mobility

Figure 13 shows 50% and 95th percentile projections with the actual deposit outline and debris scatter beyond. This shows that the actual runout L_O (distance from the slope toe) of 133 m appears to be approximately double the 95th percentile for the Whittall (2015) Optimised Mobility Index and about 10 m past the 95th percentile for the Whittall (2015) Fahrböschung Volume relationship. Individual debris particles have been scattered to 152 m, approximately another 20 m beyond the debris pile.

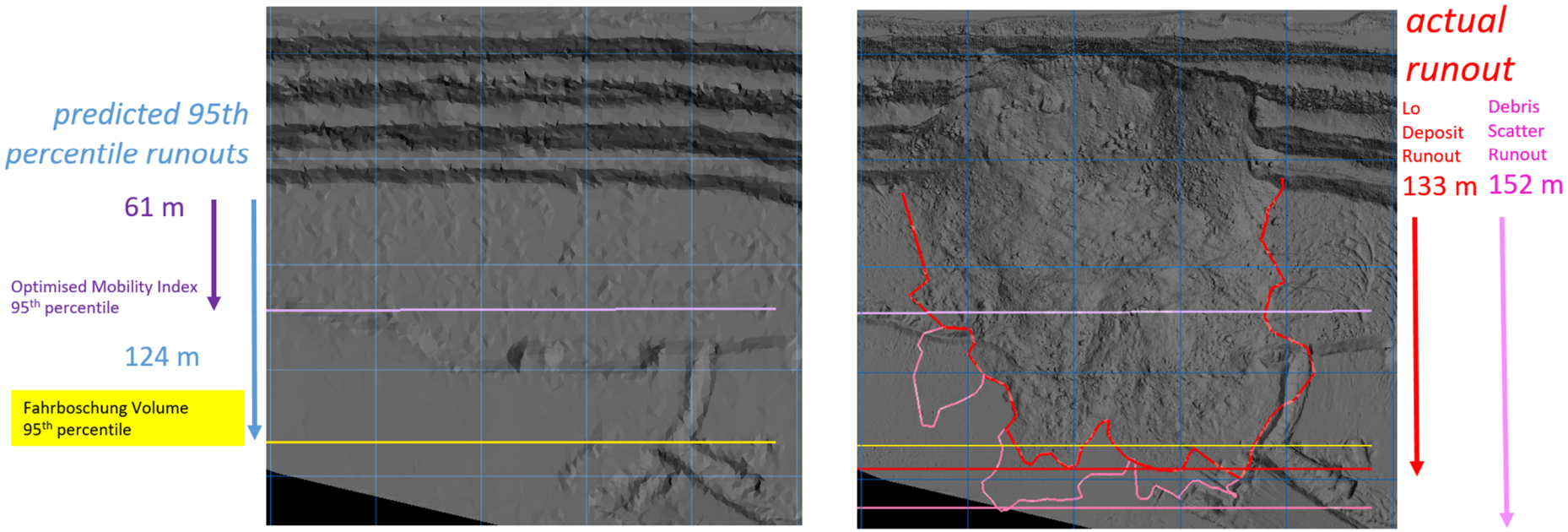

Assumes 80 m high failure, 14,000 m^2 surface area, pit crest to slope toe angle 50 degrees

Whittal, J.R., (2015) Runout Exceedance Prediction for Open Pit Slope Failures, Master of Applied Science Thesis, Geological Engineering, University of British Columbia, Vancouver.

Figure 13 Comparison between estimated and actual 95th percentile Fahrböschung Volume and Optimised Mobility Index runouts

6 Discussion

6.1 Suitability of the Fahrböschung Volume and the Optimised Mobility Index in similar Pilbara Cenozoic materials

The Optimised Mobility Index is based on a combination of data from weak weathered rock and fresh strong rock failures with a less mobile character. The Fahrböschung Volume model's weak weathered rock relationship is based only on weak weathered rock and some soils. It is to be expected, therefore, that the Optimised Mobility Index gives rise to smaller travel distance estimates. It can be concluded that use of this relationship in the soil-like materials in this environment is not appropriate.

The failure also plots as beyond the 5% runout probability exceedance in the Fahrböschung Volume model's relationship. The runout approximately coincided with the 5% runout probability exceedance for the +100% volume sensitivity case. However, individual debris clasts with the capacity to impact still travelled further. Such needs to be considered by individuals setting stand-offs.

It is difficult to conclude whether the surface water on the pit floor played a role in the runout, given the shallow depth; however, until proven otherwise, it would be prudent to assume that the models are not fit for purpose for failures onto shallow surface water. It is also important to recognise that the Whittall (2015) Fahrböschung Volume and the Whittall Optimised Mobility Index relationship do not cover potential impacts of seiche waves (tsunamis) where pits fail into water.

6.2 Are the Pilbara Cenozoic materials more mobile than the Whittall dataset?

The event clearly plots as having a probability of <5% exceedance on the Whittall (2015) Fahrböschung Volume relationship and exceeds the Whittall (2015) Optimised Mobility Index prediction by a very large margin (Figures 11 and 12). Although not explored here, one wonders what the runout would have been if the full pit floor was flat without a 4 m high flitch to cross.

Some commodities, such as coal, have material specific relationships such as that by McQuillan et al. (2018); however, the single point provided by this failure or even a collection of a few points based on Pilbara Cenozoic failures would not be statistically valid in isolation. On an individual level, the author has one data point with a 50th percentile Fahrböschung angle of 21° and is unable to estimate the 95th percentile for the Pilbara Cenozoic materials with any reliability. This is the only large failure in these materials in BHP Western Australia Iron Ore large operations. Whittall (2015) references three failures in similar iron ore mines in the same Pilbara region (partly described by Day & Seery [2007] and by Venter et al. [2013]). These failures were bedding and/or structurally controlled in Archean units. Interestingly, one of those failures, at Tom Price on a polished shale band parallel to bedding, had an Optimised Mobility Index of greater than 1, greater than the subject failure of this paper.

At the current rates of failure and the rates of publications of failures, it is likely to be many, many years – if ever – before a Pilbara Cenozoic specific relationship is available.

6.3 Use of moving surface area as a predictor of volume and hence runout

The intent of this section is to illustrate that runout estimates could change quickly where failures expand rapidly. In some cases, it could be that operations have insufficient time to adjust corresponding standoff distances suitably quickly.

Please note that for this failure, the following may be misleading, as the radar data has not been interpreted to lower displacement levels within the accuracy of the radar capability. That may well return larger surface areas if performed. Practitioners must choose their own thresholds to define moving area.

Surface area of the moving area is an input to derive failure volume, which in turn is used for the prediction of runout distance intervals.

Figure 14 shows IDS radar images of displacement ≥5 mm over 3-hour time segments in the 11 hours leading up to failure. Table 3 shows indicative surface areas of displacement ≥5 mm over 3-hour time segments, carrying through to predict a 95th percentile runout. The point of this section is to show that runout estimates increase very quickly where failures expand rapidly, and practitioners need to be aware of this.

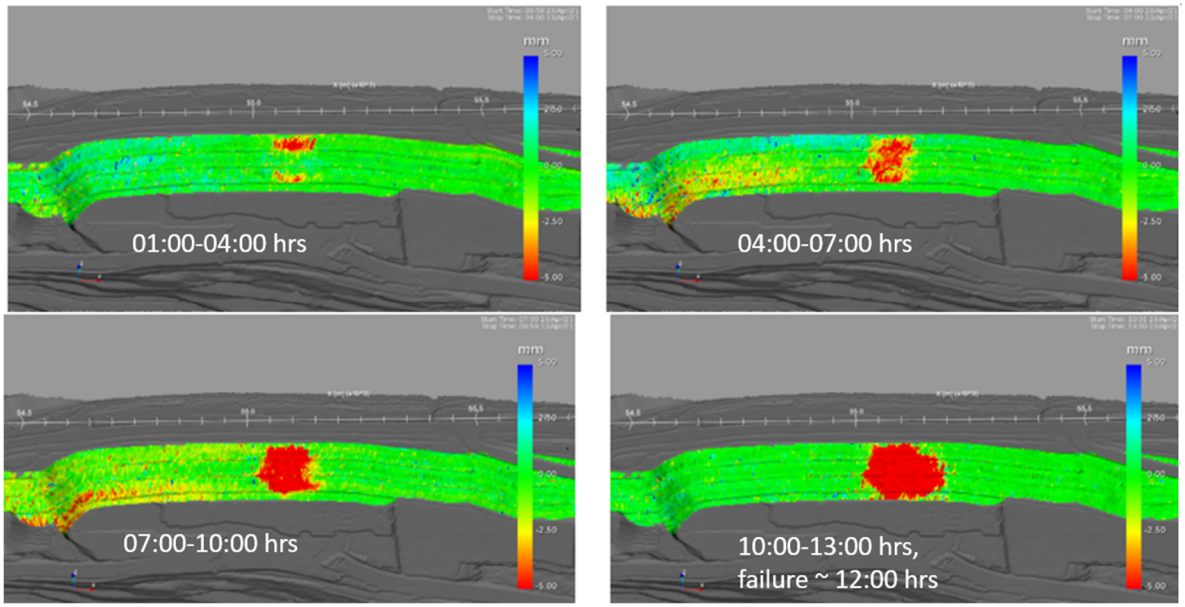

Figure 14 IDS radar data in 11 hours up to failure illustrating extent of ≥5 mm displacement at 3-hour time intervals

Table 3 Rapid change in runout estimates if displacement ≥5 mm surface area used to predict failure volume

Time before failure	Indicative surface area moving ≥5 mm displacement (m^2)	95th percentile runout estimate Whittall (2015) Optimised Mobility Index (m)	95th percentile runout estimate Whittall (2015) Fahrböschung Volume (m)
8 hours	3,500	38	79
5 hours	7,000	48	100
2 hours	11,500	57	115
Failure	14,000	61	124

6.4 Hydrogeology

It is interpreted that water played a part in the failure, given the evidence of local seepages. The wet pit floor could have contributed to the runout due to reduced friction.

It is not possible to draw conclusions with high confidence due to incomplete data; however, the following discussion may serve some purpose in highlighting uncertainties and limitations, even when monitoring is available.

6.4.1 Lack of groundwater data within the slope

Vibrating wire piezometer, if installed using a low permeability grout, can theoretically measure different porewater pressures in different units, including those of low permeability. Open standpipes do not have this ability.

If vibrating wire piezometer sensors had been installed below the interpreted pre-mining groundwater level, they would not have been able to measure the pressure effects of rainfall moving through the slope

above the interpreted pre-mining groundwater table. Transient pressures have been reported in piezometers above the water table at other sites (Lorig et al. 2013 quoting Ida Bagus Donni Viriyatha). Such installations and regular monitoring would be helpful in future to better understand hydrogeology.

However, even if installed, there may be limitations such that the pressure effects of rainfall moving through vibrating wire piezometers fully grouted above the interpreted pre-mining groundwater table may or may not be identified. In addition, even with such installations, different pressures could be occurring in other parts of the slope than at the monitored location. This is illustrated by the localised presentation of seepage on the face. Furthermore, the failure was relatively shallow, and it is not always practical to monitor that part of the slope close to the pit face.

7 Conclusion

It is concluded that a slope failure in Cenozoic materials in the Pilbara travelled with a Fahrböschung angle of 21°. This exceeded the 95th percentile travel distance prediction of the Whittall (2015) Optimised Mobility Index model by a very large amount and exceeded the Whittall (2015) Fahrböschung Volume 95th percentile travel distance prediction.

The slope did fail onto surface water (unmeasured but estimated as approximately 10 cm, with some islands, based on photographs). It is not clear to what extent this influenced the runout.

There is insufficient data to make a Pilbara Cenozoic specific runout model.

It is clear that the Optimised Mobility Index is not appropriate for soil or weathered weak rock, as it is based on a dataset containing a significant portion of less mobile fresh strong rock.

Practitioners setting stand-offs in the Pilbara Cenozoic environment described by Baxter (2016) must do as they see fit; however, the author would not feel comfortable to set stand-offs based on the Fahrböschung Volume models in such environments until further data is captured.

Acknowledgement

I would like to thank all staff at BHP West Australian Iron Ore, both past and present, who have contributed, in particular Arturo Maldonado.

I would also like to thank J Whittall, for offering empirical relationships based on real data to set stand-offs.

References

Baxter, H 2016, 'Geophysics, geochemistry and engineering geology: how disciplines combine to improve mine slope design in the Pilbara detrital valleys of Western Australia', in MJ Eggers, JS Griffiths, S Parry & MG Culshaw (eds), *Developments in Engineering Geology*, Engineering Geology Special Publication 27, Geological Society, London, pp. 81–92 http://doi.org/10.1144/EGSP27.7

Day, AP & Seery, JM 2007, 'Monitoring of a large wall failure at Tom Price iron ore mine', in Y Potvin (ed.), *Slope Stability 2007: Proceedings of the 2007 International Symposium on Rock Slope Stability in Open Pit Mining and Civil Engineering*, Australian Centre for Geomechanics, Perth, pp. 333–340, https://doi.org/10.36487/ACG_repo/708_20

Lorig, L, Dowling, J, Beale, G & Royle, M 2013, 'Numerical model', in G Beale & J Read (eds), *Evaluating Water in Pit Slope Stability*, CSIRO Publishing, Melbourne, pp. 216–277.

McQuillan, A, Canbulat, I, Payne, D, Oh, J 2018, 'New risk assessment methodology for coal mine excavated slopes', *International Journal of Mining Science and Technology*, vol. 28, no. 201, pp. 583–592.

Venter, J, Kuzmanovic, A & Wessels, SDN 2013, 'An evaluation of the CUSUM and inverse velocity methods of failure prediction based on two open pit instabilities in the Pilbara', in PM Dight (ed.), *Slope Stability 2013: Proceedings of the 2013 International Symposium on Slope Stability in Open Pit Mining and Civil Engineering*, Australian Centre for Geomechanics, Perth, pp. 1061–1076, https://doi.org/10.36487/ACG_rep/1308_74_Venter

Whittall, JR 2015, *Runout Exceedance Prediction for Open Pit Slope Failures*, MSc thesis, The University of British Columbia, Vancouver.

Whittall, J, Mitchell, A & McDougall, S 2020, 'Runout of open pit slope failures: an update', in PM Dight (ed.), *Slope Stability 2020: Proceedings of the 2020 International Symposium on Slope Stability in Open Pit Mining and Civil Engineering*, Australian Centre for Geomechanics, Perth, pp. 1149–1162, https://doi.org/10.36487/ACG_repo/2025_76